Science Advances

AAAS

advances.sciencemag.org/cgi/content/full/2/11/e1601542/DC1

Supplementary Materials for

How will induced seismicity in Oklahoma respond to decreased saltwater injection rates?

Cornelius Langenbruch and Mark D. Zoback

Published 30 November 2016, *Sci. Adv.* **2**, e1601542 (2016)
DOI: 10.1126/sciadv.1601542

This PDF file includes:

- Supplementary Methods
- fig. S1. Maximum magnitude expected during 1900 years of tectonic earthquake activity in Oklahoma.
- fig. S2. Saltwater injection and earthquake rate in CO.
- fig. S3. Saltwater injection and earthquake rate in WO.
- fig. S4. Observation and prediction of induced seismicity in CO.
- fig. S5. Observation and prediction of induced seismicity in WO.
- fig. S6. Annual magnitude exceedance probability and maximum magnitude in CO.
- fig. S7. Annual magnitude exceedance probability and maximum magnitude in WO.
- fig. S8. Annual magnitude exceedance probability and maximum magnitude.
- fig. S9. Cumulative magnitude exceedance probability and maximum magnitude in CO and WO (2009 to September 2016).
- table S1. Recent magnitude 4.5 and larger earthquakes in Oklahoma.
- References (*28*, *29*)

Supplementary Methods

method S1. Computation of the pressure rate shown in Fig. 3

The red dashed line in Fig. 3 shows the normalized pressure rate 3km below the injection interval (corresponding to the average depth of the earthquake hypocenters). It was computed according to 3D diffusion and reported saltwater injection rates for all Arbuckle injection wells in central and western Oklahoma. Considering a point like fluid injection of duration t_0 and constant source pressure P_0 into a homogeneous, isotropic and fluid saturated 3D medium the pressure at time t and distance r to the injection point is given by (*28*) as

$$p(r,t) = \frac{P_0}{4\pi rD} erfc\left(\frac{r}{\sqrt{4Dt}}\right), \quad t \le t_0 \tag{S1}$$

$$p(r,t) = \frac{P_0}{4\pi rD}\left(erfc\left(\frac{r}{\sqrt{4Dt}}\right) - erfc\left(\frac{r}{\sqrt{4D(t-t_0)}}\right)\right), t > t_0 \tag{S2}$$

D corresponds to the hydraulic diffusivity of the rock and erfc is the complementary Gaussian error function. Each Arbuckle injection well in Oklahoma was considered as a point source. The source pressure P_0 at the individual wells correspond to a boxcar function switched on at the beginning of each month and switched of the end of each month. The height of the boxcar (the source pressure P_0) corresponds to the fluid injection rate during the considered month at the considered well.

Using a diffusivity of D=0.08 m^2/s (≈1 mD permeability) we computed the pressure at 10000 randomly selected points on a layer 3km below the injection interval (corresponding to the average depth of the earthquake hypocenters). The chosen diffusivity value is in agreement with values reported for the crystalline basement at enhanced geothermal systems (*29*). Each location in central and western Oklahoma had the same probability to be selected as a point for pressure computation. The 10000 randomly selected points can be considered as the locations of 10000 preexisting fractures. Since the location of fractures in the basement is not known a random fracture location distribution was a reasonable assumption.

Using the pressure computed according to eqs. S1 and S2 the pressure rate (the temporal derivative of the pressure) at each randomly selected point (the locations of preexisting fractures) was computed. Increasing pressure (a positive pressure rate) resulting from injection reduces the frictional resistance to sliding and can trigger the release of the accumulated stress in earthquakes. The red dashed line in Fig. 3 shows the summation of all positive pressure rates at all preexisting fracture. Negative pressure rates (corresponding to a decreasing pressure) were not considered, because they increase the effective normal stress at the preexisting fractures and result in fracture strengthening.

method S2. Computation of Omori's law shown in Fig. 4

To describe the decay of seismicity after injection, we followed (13) and utilized a modification of Omori's law, describing the decay of aftershock sequences of large tectonic earthquakes

$$R(t) = \frac{R_0}{(\frac{t}{t_0})^p}, \quad t > t_0 \tag{S3}$$

t_0 corresponds to the length of a considered fluid injection (above the triggering threshold), R(t) is the seismicity rate at time t (from injection start) for $t > t_0$. R_0 corresponds to the seismicity rate at injection stop (or a significant decrease of the injection rate) and p is the p-value of Omori's law describing the rate of the decay. In agreement with the conceptual model of other studies analyzing induced seismicity in Oklahoma, eq. S3 has been derived based on the concept that the triggering mechanism of induced seismicity is pore pressure diffusion in the pore and fracture space of rocks from the injection wells to preexisting faults near failure. Eq. 3 states that seismicity caused by short term fluid injection (e.g. for hours) will decay within the same timescale (within hours). Seismicity caused by fluid injection (above the triggering threshold) for years can require years to decay completely. Omori's law shown in Fig. 3 was computed according to eq. S3. Because saltwater has been injection significantly above the seismicity triggering threshold in both central and western Oklahoma for approximately two years before the injection rates start to decrease significantly we used t_0=2 years for the computation. Moreover, a p-value of p=2 was used for computation of Omori's law shown in Fig. 4. We note that the assumption of a p-value of p=2 represents a conservative decay rate (13). The decay of seismicity observed after injection at enhanced geothermal systems usually is characterized by larger p-values. The

results in Figs. 4 and 5 can be updated during the next year or two if the seismicity decays faster than assumed.

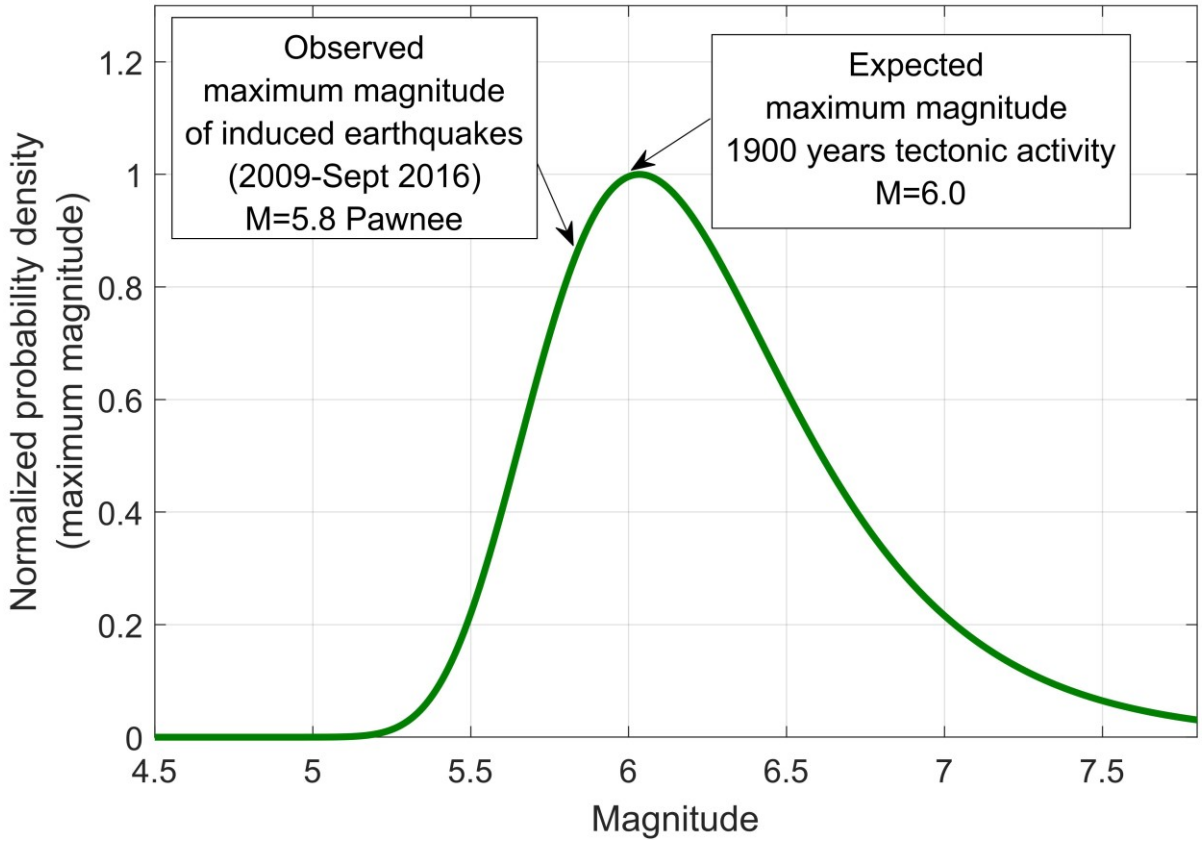

fig. S1. Maximum magnitude expected during 1900 years of tectonic earthquake activity in Oklahoma. The probability distribution was computed based on the average annual number of earthquakes observed between 1979 and 2009 in complete Oklahoma (1.16 earthquakes $M \geq 3$ and $1.16 * 10^{-b(M-3)}$ earthquakes of magnitude M and larger). The maximum likelihood estimate of the b-value of the tectonic background activity (1979 and 2009) is b=1.1 (for more details see section "Magnitude exceedance probability" in the main text.

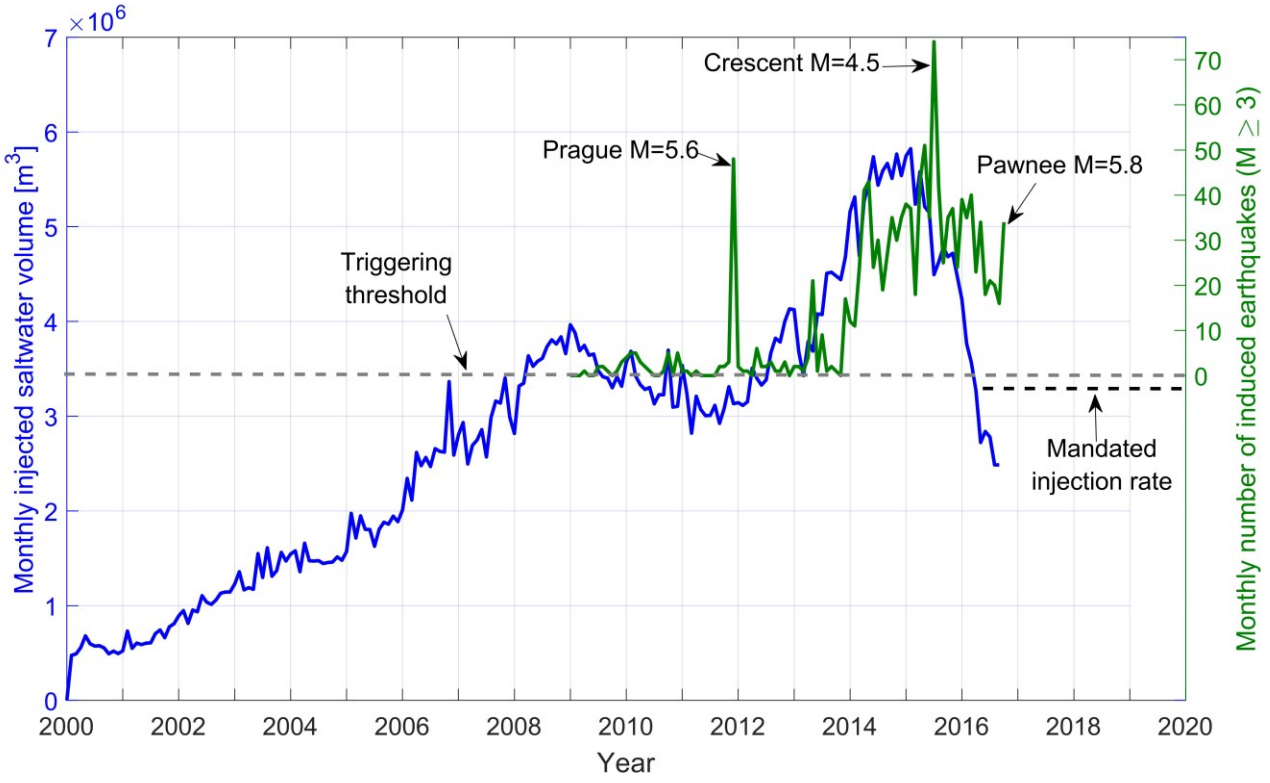

fig. S2. Saltwater injection and earthquake rate in CO. Monthly Arbuckle saltwater injection (blue line) and earthquake rate (green line). The seismicity triggering threshold of the injection rate was determined by calibration of the SI model. Aftershock sequences are visible in the monthly earthquake rates for the largest magnitudes. The mandated injection rate corresponds to 60% of the total volume injected in 2014.

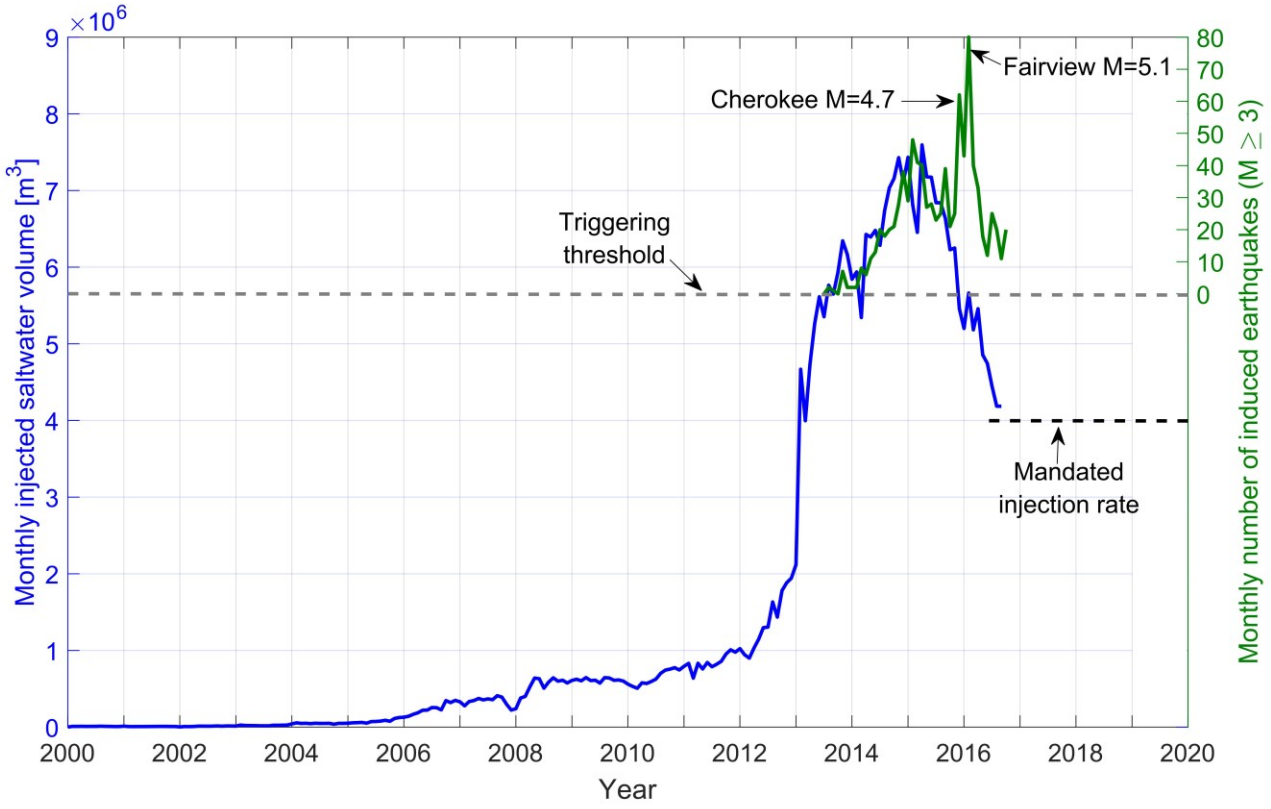

fig. S3. Saltwater injection and earthquake rate in WO. Monthly Arbuckle saltwater injection (blue line) and earthquake rate (green line). The seismicity triggering threshold of the injection rate was determined by calibration of the SI model. Aftershock sequences related to four M 4.7+ earthquakes between November 2015 and February 2016 delay the decay of the induced earthquake sequence. The mandated injection rate corresponds to 60% of the total volume injected in 2014.

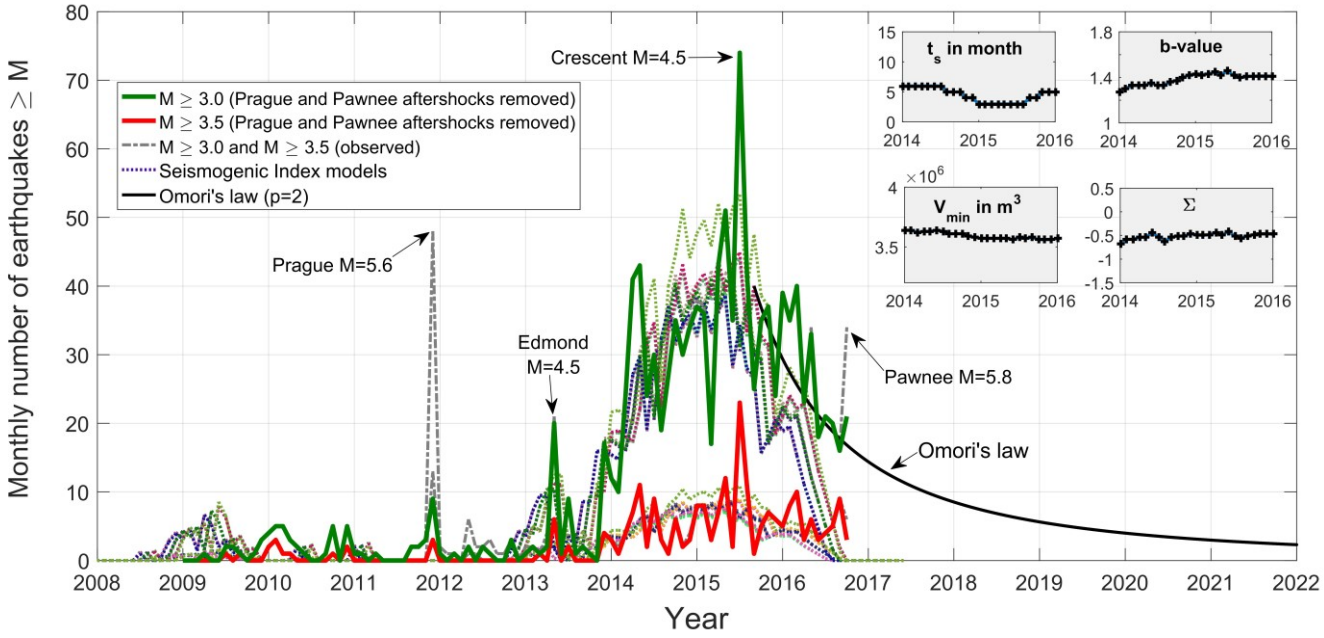

fig. S4. Observation and prediction of induced seismicity in CO. Solid colored lines show the monthly number of observed earthquakes ($M \geq 3$ green, $M \geq 3.5$ red) in CO (aftershocks of $M \geq 4.7$ events have been removed). The gray dashed lines present the complete earthquake catalog. The colored dotted lines show SI models calibrated through different times between June 2014 and December 2015. Parameter of the SI models calibrated until different times are shown in the insets of the figure. The black solid line shows a decay of $M \geq 3$ earthquakes according to Omori's law (p=2).

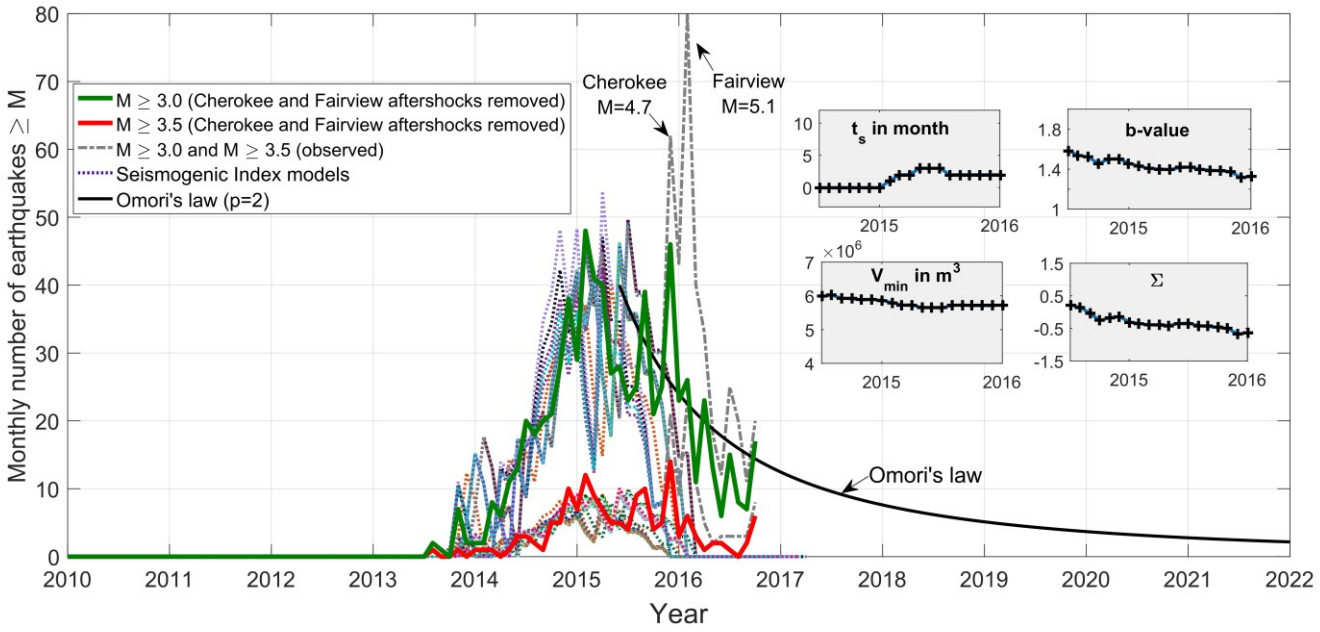

fig. S5. Observation and prediction of induced seismicity in WO. Solid colored lines show the monthly number of observed earthquakes ($M \geq 3$ green, $M \geq 3.5$ red) in WO (aftershocks of $M \geq 4.7$ events have been removed). The gray dashed lines present the complete earthquake catalog. The colored dotted lines show SI models calibrated through different times between June 2014 and December 2015. Parameter of the SI models calibrated until different times are shown in the insets of the figure. The black solid line shows a decay of $M \geq 3$ earthquakes according to Omori's law (p=2).

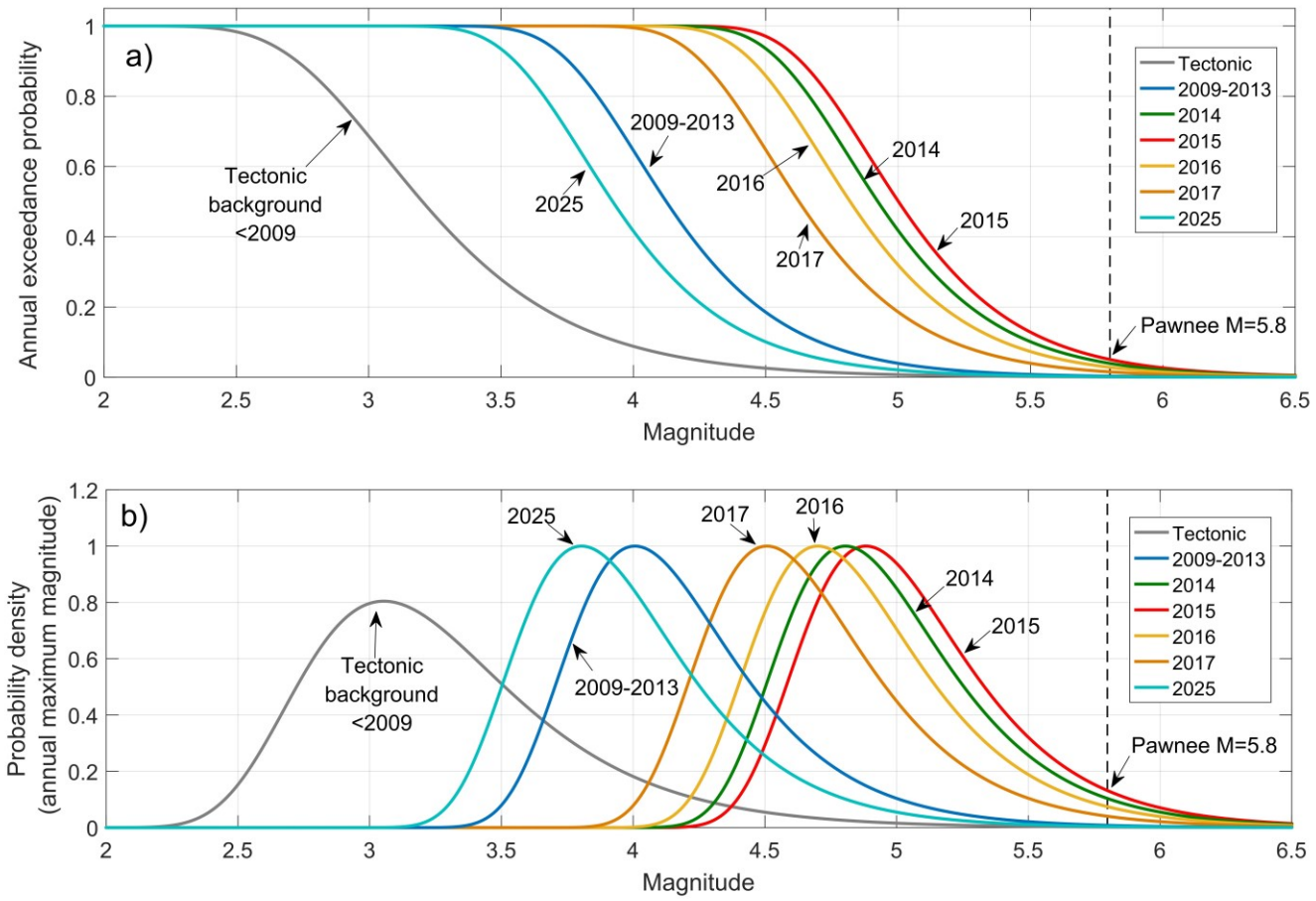

fig. S6. Annual magnitude exceedance probability and maximum magnitude in CO. The figure shows annual probabilities of exceeding magnitude M (**a**) and the maximum magnitude (**b**) in CO. Magnitude exceedance probabilities have been computed according to Eq. 2 as well as assuming the applicability of Omori's law to describe the decay of seismicity following injection. The probability distribution of the maximum magnitude corresponds to the magnitude derivative of the exceedance probability. Due to the high saltwater injection rates the probability of potentially-damaging earthquakes is enhanced compared to the tectonic activity and critically high in 2014, 2015 and 2016.

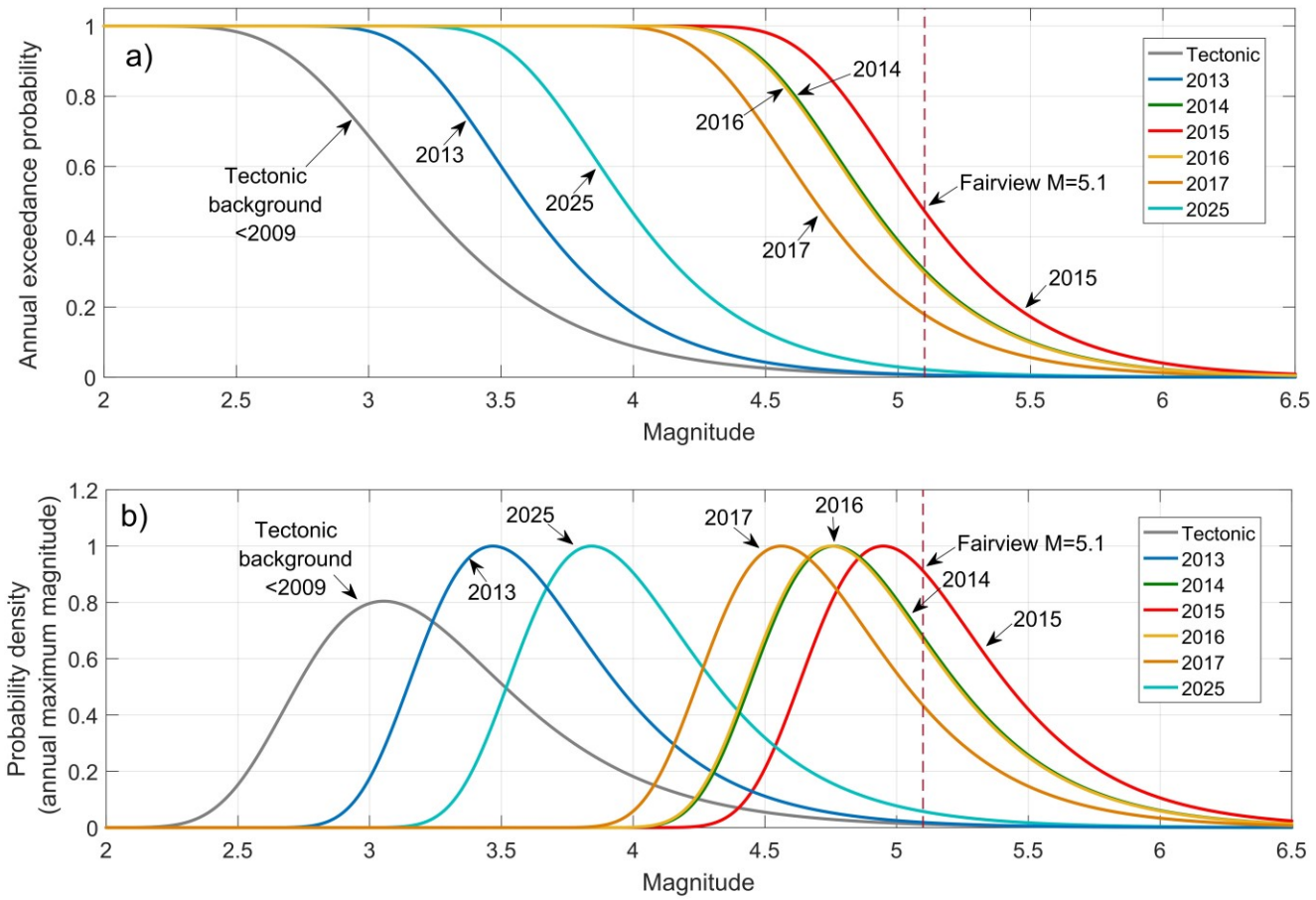

fig. S7. Annual magnitude exceedance probability and maximum magnitude in WO. The figure shows annual probabilities of exceeding magnitude M (**a**) and the maximum magnitude (**b**) in WO. Magnitude exceedance probabilities have been computed according to Eq. 2 as well as assuming the applicability of Omori's law to describe the decay of seismicity following injection. The probability distribution of the maximum magnitude corresponds to the magnitude derivative of the exceedance probability. Due to the high saltwater injection rates the probability of potentially-damaging earthquakes is enhanced compared to the tectonic activity and critically high in 2014, 2015 and 2016.

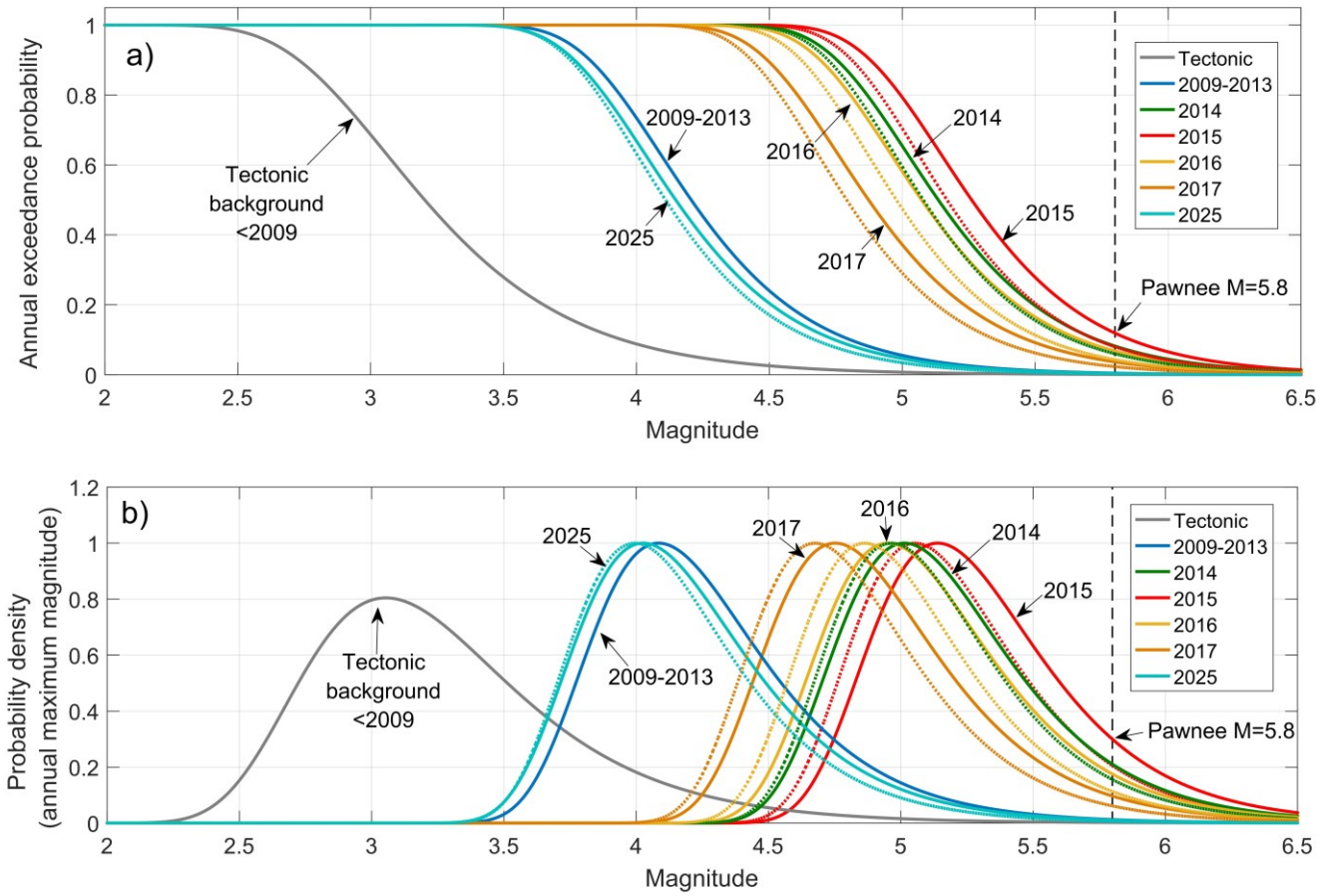

fig. S8. Annual magnitude exceedance probability and maximum magnitude. The figure shows annual probabilities of exceeding magnitude M (**a**) and the maximum magnitude (**b**) in the combined area of CO and WO. Solid lines correspond to the SI model calibrated through December 2015 and dotted lines show the probabilities based on model calibration through June 2014. Magnitude exceedance probabilities have been computed according to Eq. 2 as well as assuming the applicability of Omori's law to describe the decay of seismicity following injection. The probabilities change only slightly and could have been assessed in the early phase of the induced earthquake sequence.

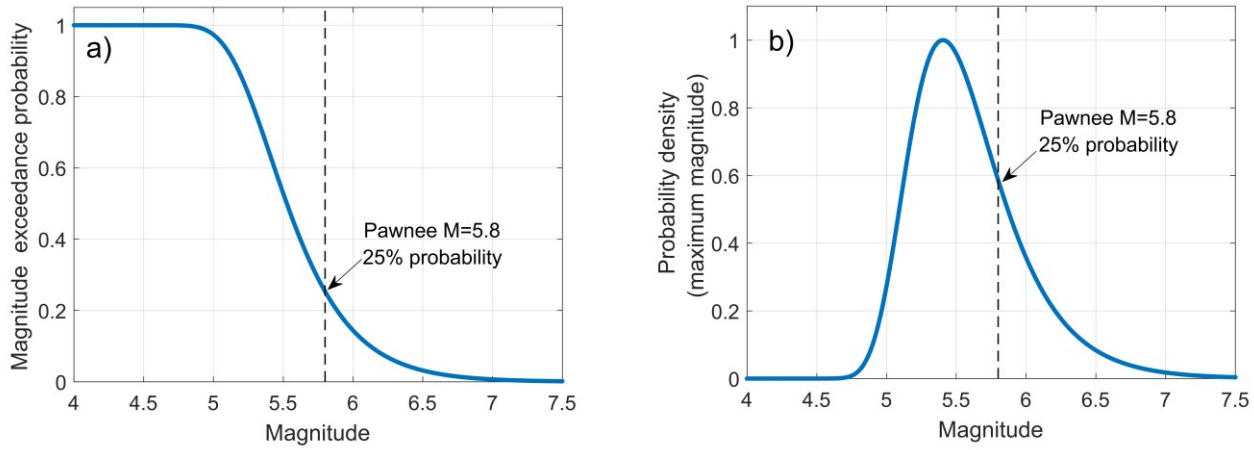

fig. S9. Cumulative magnitude exceedance probability and maximum magnitude in CO and WO. The figure shows probabilities of exceeding magnitude M (**a**) and the maximum magnitude (**b**) during the time from 2009 to September 2016. The probability distribution of the maximum magnitude correspond to the magnitude derivative of the exceedance probability. The probability to exceed M=5.8 (Pawnee) by injection of saltwater (2009 - September 2016) is 25%.

table S1. Recent magnitude 4.5 and larger earthquakes in Oklahoma. The table includes all M 4.5 and larger earthquakes in Oklahoma between 2009 and September 2016. Note that all M 4.5+ earthquakes in WO occur after the injection rates have already been significantly decreased.

Magnitude	Epicenter location	Occurrence time
5.1	(WO) 31km NW of Fairview	2016-02-13 17:07:06 UTC
4.7	(WO) 33km NW of Fairview	2016-01-07 04:27:57 UTC
4.7	(WO) 26km E of Cherokee	2015-11-30 09:49:12 UTC
4.7	(WO) 13km SW of Cherokee	2015-11-19 07:42:12 UTC
5.8	(CO) 14km NW of Pawnee	2016-09-03 12:02:44 UTC
4.5	(CO) 4km NNE of Crescent	2015-07-27 18:12:15 UTC
4.5	(CO) 9km ESE of Edmond	2013-12-07 18:10:24 UTC
4.8	(CO) Prague	2011-11-08 02:46:57 UTC
5.6	(CO) Prague	2011-11-06 03:53:10 UTC
4.8	(CO) Prague	2011-11-05 07:12:45 UTC